High-Bandwidth Suspension Resonance Analysis of In-Wheel Motor Vehicle Using Multibody Dynamics

Tomonori Suzuki
Graduate School of Frontier Science
The University of Tokyo
Chiba, Japan
tomonorisuzuki@ieee.org

Fabien Chauvicourt
Engineering Consulting Services
Siemens Industry Software NV
Leuven, Belgium
Fabien.chauvicourt@siemens.com

Hiroshi Fujimoto
Graduate School of Frontier Science
The University of Tokyo
Chiba, Japan
fujimoto@k.u-tokyo.ac.jp

***Abstract*—Vibration suppression control of vehicles is important for ride comfort. In vehicles electrification, the in-wheel motor as an actuator for vibration suppression has attracted attention as an alternative to active suspension systems. For controller design, it is necessary to figure out the characteristics of the system. However, the frequency response characteristics of the suspension with the in-wheel motor are not fully understood. A conventional and traditional quarter car model gives an expression of only two resonances of the suspension system. This paper reveals that the third resonance comes from the suspension bushing using multibody dynamics. The authors also perform a sensitivity analysis of the frequency responses for a set of bushing stiffnesses that may differ with the product lifetime. Lastly, the authors show a feedforward controller design example based on the model analysis.**

***Index Terms*—in-wheel motor, suspension, bushing, high-bandwidth resonace, multibody dynamics.**

I. Introduction

In recent years, electric vehicles (EVs) have attracted much attention as a result of increasing environmental awareness. EVs have high motion performance because of their motor characteristics. Electric motors have three significant advantages over internal combustion engines: their torque response is several hundred times faster and more accurate than that of the internal combustion engine, their output torque can be directly measured from the current value of the motor, and distributed small motors enable flexible arrangements [1]. By utilizing these features effectively, advanced vehicle motion control becomes possible [2]–[4].

In particular, the distributed arrangement of motors enables various drivetrain configurations in EVs. One such configuration is an in-Wheel Motor (IWM) system in which motors are mounted in each wheel. The IWM system has the advantages of reducing the total weight of a drivetrain and increasing the freedom of interior layout design [5]. From a control perspective, torque-vectoring enables higher motion performance, and the shorter driveshaft removes low-frequency resonances that create a substantial limitation in control [6], [7].

To improve motion performance and ride comfort, several vibration suppression control methods which target several Hz bands have been proposed [8]–[10]. However, the IWM system increases the unsprung weight and causes deterioration of ride comfort over 4 Hz [11], [12]. To solve this problem, studies

Fig. 1. Experimental vehicle overview.

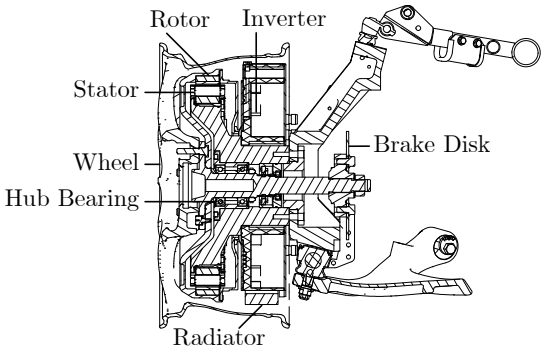

Fig. 2. In-wheel motor unit overview.

on vibration suppression for the unsprung vertical axis mode and the longitudinal axis mode that lie in a higher frequency band (10 Hz and above) have been conducted [13]–[15].

These vibration suppression control methods at high bandwidths use the high torque responsiveness of the IWM system. As described above, extensive research using the IWM system has been carried out to suppress vibration in a wide frequency range [16].

It is essential to identify the frequency response characteristics from the motor to the vertical acceleration of the sprung

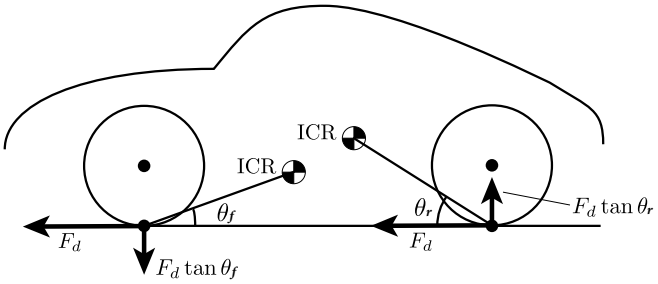

Fig. 3. Suspension reaction force.

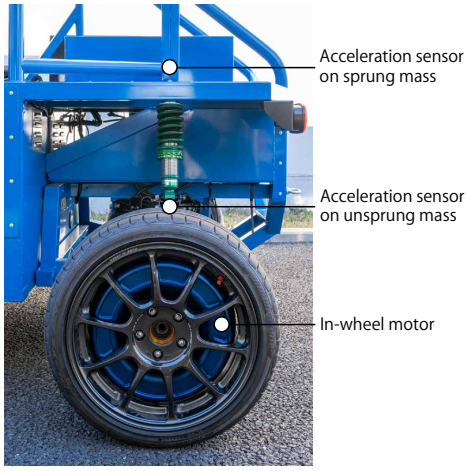

Fig. 4. Experimental vehicle system identification.

mass in such a controller design. Some resonance exists in the IWM vehicle's frequency response [15], and resonance causes instability and bandwidth limitation of the control. However, only two resonances from lower frequency were revealed using the traditional quarter model. It is necessary to reveal the cause of high bandwidth resonance for more high-performance motion control.

This paper reveals the cause of the third resonance using the multibody dynamics model. In section II, we identified the frequency response characteristics of the experimental IWM vehicle. In section III, we describe the conventional quarter car model and confirm the limitation of the conventional model. In section IV, we provide the multibody dynamics model of the IWM vehicle suspension and analyze the resonance cause using the proposed model. We reveal that the third resonance comes from bushing stiffness. In section V, we show a feedforward controller design example based on the model analysis.

II. System Identification with Experimental Vehicle

A. Experimental vehicle

We use the experimental vehicle shown in Fig. 1. The experimental vehicle is rear-wheel drive and has IWM units in rear wheels shown in Fig. 2. The IWM unit consists of a

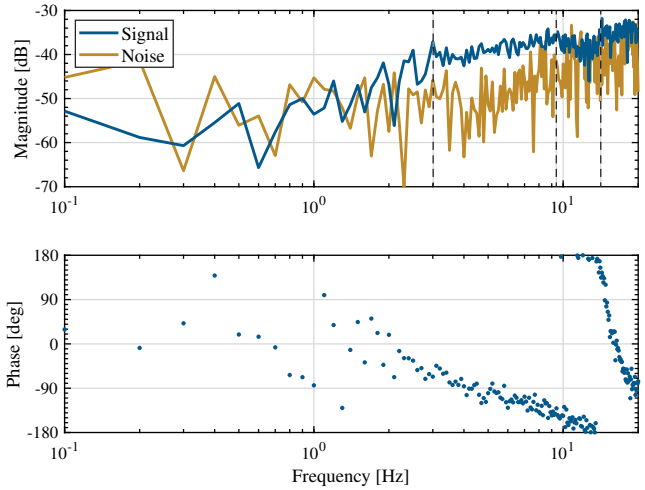

Fig. 5. Frequency response of sprung mass vertical acceleration of experimental vehicle.

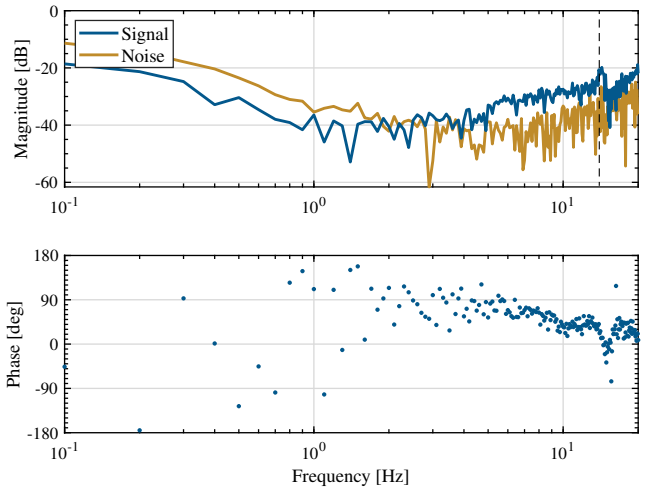

Fig. 6. Frequency response of unsprung mass vertical acceleration of experimental vehicle.

motor, an inverter, and a radiator. The rear suspensions are standard double wishbone suspensions. The double wishbone suspension is a suspension design that uses two parallel wishbone-shaped arms to locate the wheel. The experimental vehicle is equipped with acceleration sensors on the sprung and unsprung mass at the rear left wheel for the analysis. The frequency response from motor torque to the sprung mass acceleration is analyzed in the following sections.

B. Suspension reaction force

The suspension reaction force F_c is defined as the vertical component of the internal suspension forces caused by the driving forceF_d. By driving the IWM with pre-defined torque, a suspension reaction force appears and generates a vertical acceleration of the unsprung mass.

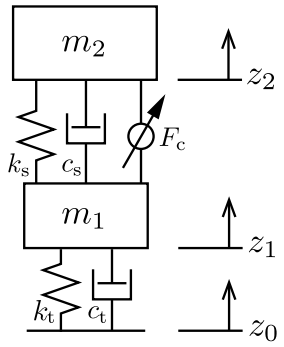

Fig. 7. Quarter car model.

Fig. 3 shows the lateral view of the simplified kinematic model of a vehicle with suspension reaction forces. The arm between the sprung and unsprung masses has a structure that rotates around the instant center of rotation (ICR). ICR is determined by the suspension structure and regarded as constant. The driving force working on the tire in the longitudinal direction causes a moment in the arm about the ICR. The vertical force that balances the moment of the driving force is then generated.

Assuming that the angle between the ground and ICR of the arm is θ, the magnitude of the driving force is F_d, the slip ratio is a constant, the suspension reaction force F_c in the vertical direction can be calculated as follows:

$$F_\mathrm{c} = F_\mathrm{d} \tan\theta = rT \tan\theta. \tag{1}$$

C. System identification of experimental vehicle

We identify the frequency response from the rear wheel motor torque to the vertical acceleration using a multi-sine signal [17]. Multi-sine signal $u(t)$ is expressed as:

$$u(t) = \sum_{k=1}^{N} A_k \sin(w_k t + \phi_k), \tag{2}$$

where t denotes continuous time, A_k denotes amplitude, w_k denotes angular frequency, ϕ_k denotes phase for $k = 1, \ldots, N$.

A multi-sine signal consists of the sum of the discrete frequency sine waves. Therefore, the output spectrum of the frequency that the multi-sine input signal does not have is considered non-linear characteristics. Because we identified the plant as a linear system, the non-linear characteristics are considered as noise. S/N ratio can be calculated using a multi-sine signal.

We measured the vertical acceleration of both the sprung and the unsprung mass of the rear left wheel shown in Fig. 4. We applied the same multi-sine input torque to the two rear wheel motors and released the front wheels' brakes. The amplitude of the input torque is $150\,\mathrm{Nm}$; the duration is $200\,\mathrm{s}$. The identified frequency range is from $0.1\,\mathrm{Hz}$ to $20\,\mathrm{Hz}$ in $0.1\,\mathrm{Hz}$ increments.

The identified frequency response from motor torque to sprung and unsprung mass acceleration are displayed in Fig. 5 and Fig. 6. The essential frequency characteristics are the sprung mass's vertical acceleration because it mostly affects the ride comfort. This frequency characteristic has three main resonances. The first resonance is around $3\,\mathrm{Hz}$, the second resonance is around $9\,\mathrm{Hz}$, and the third resonance is around $14\,\mathrm{Hz}$.

TABLE I
VEHICLE MODEL PARAMETER DEFINITIONS.

Symbol	Meaning
m_1	Quarter unsprung mass
m_2	Quarter sprung mass
k_s	Spring stiffness
c_s	Damping coefficient
k_t	Tire stiffness
c_t	Tire damping coefficient
z_0	Road displacement
z_1	Unsprung mass displacement
z_2	Sprung mass displacement
F_d	Driving force
θ	Angle of instant suspension rotation
F_c	Suspension reaction force
r	Radius of tire
T	Motor torque

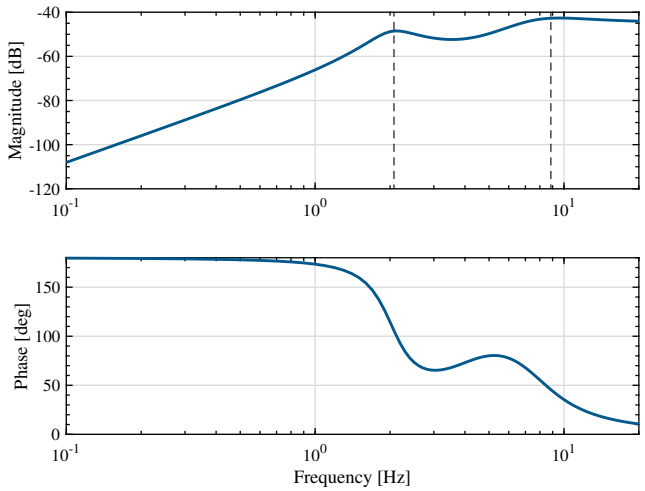

Fig. 8. Frequency response of sprung mass vertical acceleration of quarter car model.

III. Conventional Analysis Using Quarter Car Model

The vertical vehicle vibration is traditionally analyzed by the quarter car model, as shown in Fig. 7. This model consists of a quarter sprung mass, a quarter unsprung mass, suspension, and a tire. The definition of each variable is shown in Table I. F_c is a suspension reaction force.

The motion equations of the quarter car model are given as follows:

$$m_2 z_2 s^2 = (c_\mathrm{s} s + k_\mathrm{s})(z_1 - z_2) + F_\mathrm{c}, \tag{4}$$

$$m_1 z_1 s^2 = -(c_\mathrm{s} s + k_\mathrm{s})(z_1 - z_2) + (c_\mathrm{t} s + k_\mathrm{t})(z_0 - z_1) - F_\mathrm{c}. \tag{5}$$

$$\frac{\ddot{z}_2}{F_c} = \frac{s^2(m_1 s^2 + c_t s + k_t)}{m_1 m_2 s^4 + \{(m_1 + m_2)c_s + m_2 c_t\}s^3 + \{(m_1 + m_2)k_s + m_2 k_t + c_s c_t\}s^2 + (c_s k_t + c_t k_s)s + k_s k_t} \tag{3}$$

TABLE II
MULTIBODY SUSPENSION MODEL RIGID BODIES STRUCTURE.

Rigid body	End point 1		End point 2	
	Rigid body	Joint type	Rigid body	Joint type
Upper arm	Main body	Cylindrical Joint	Upright	Spherical joint
Lower arm	Main body	Cylindrical Joint	Upright	Spherical joint
Rod	Main body	Cylindrical Joint	Upright	Spherical joint
Wheel	Upright	Revolute joint		

TABLE III
MULTIBODY SUSPENSION MODEL STIFFNESS PARTS STRUCTURE.

Parts	End point 1	End point 2
Main spring and damper	Upright	Main body
Bush 1	Upper arm	Main body
Bush 2	Lower arm	Main body
Bush 3	Rod	Main body
Tire (vertical)	Wheel	Fixed Road
TIre (longitudinal)	Wheel	Fixed Road

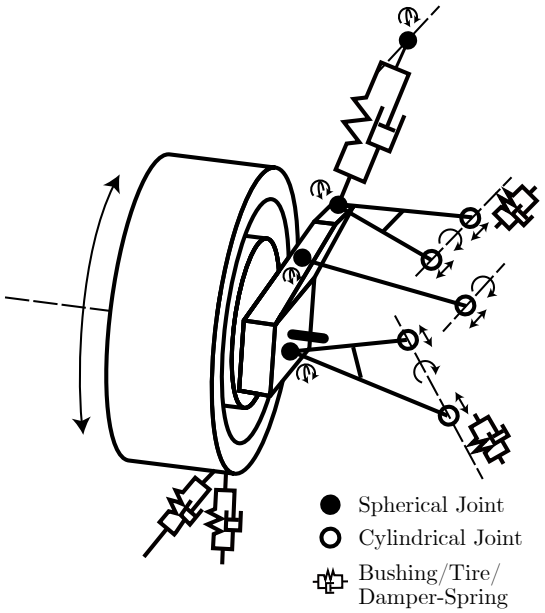

(a) Multibody dynamics model concepts.

(b) Multibody dynamics model overview.

Fig. 9. Multibody dynamics model.

The transfer function model from motor torque to the sprung mass acceleration of the quarter car model is given in (3), and its bode diagram is shown in Fig. 8.

This transfer function with experimental vehicle parameters has two resonances around 2 Hz and 9 Hz and one anti-resonance around 3 Hz.

The first resonance comes from sprung mass and suspension stiffness. The second resonance comes from unsprung mass and tire stiffness.

In the frequency response of the quarter car model, only two resonances are contained. The quarter car model cannot explain the third resonance. A more precise model should be considered.

IV. RESONANCE ANALYSIS USING MULTIBODY DYNAMICS

A. Suspension modeling using multibody dynamics

The suspension system can be modeled using multibody dynamics. A multibody dynamic model consists of solid bodies or links connected by joints that restrict their relative motion. The links have elasticity and viscosity.

The design and overview of the multibody dynamics suspension model we made are shown in Fig. 9(a) and Fig. 9(b).

This model consists of 6 rigid bodies: upper arm, lower arm, rod, upright, wheel, body. The joints connect these rigid bodies. The types of the joint are cylindrical joint, spherical joint, and revolute joint. The connections of joints between rigid body is shown as Table II.

The connected points sometimes have elasticity and viscosity, which models damper springs, tires, and bushings. The location of elasticity and viscosity is shown in Table III.

The material of the upper arm, the lower arm, the upright, and the wheel is aluminum. The material of the rod, the damper spring, and the body is steel. The bushing and tire are made of rubber.

The rigid bodies except the body have 6 degrees of freedom

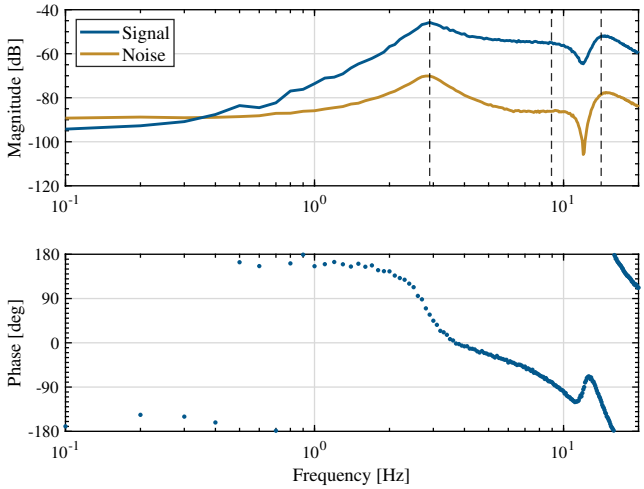

Fig. 10. Frequency response of sprung mass vertical acceleration of multibody dynamics model.

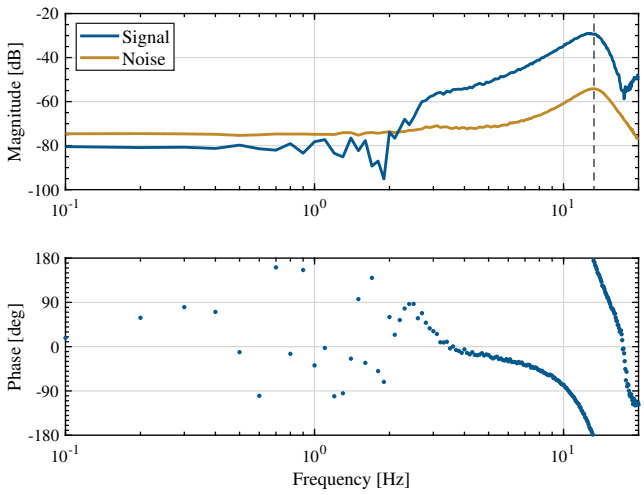

Fig. 11. Frequency response of unsprung mass vertical acceleration of multibody dynamics model.

(DOFs) of motion. The only body motion is restricted to 2 DOFs for longitudinal and vertical translation directions. The other 4 DOFs are restricted. The lateral translation, yaw, and roll motion are considered 0 because both the vehicle's side mechanism is identical. Pitch motion generated by both front and rear suspension motion is restricted in this model because it has only rear suspension.

B. System identification using multibody dynamics

Simcenter 3D Motion software is used for multibody dynamics modeling, simulation and analysis.

We identify the frequency response from the wheel motor torque to the vertical acceleration of sprung and unsprung mass using a multi-sine signal [17] as we did with the experimental vehicle. The amplitude of the input torque is $100\,\mathrm{Nm}$; the duration is $40\,\mathrm{s}$. The identified frequency response are displayed in Fig. 10 and Fig. 11. This sprung mass frequency characteristic using the multibody dynamics model has three main resonances. The first resonance is around $3\,\mathrm{Hz}$, the second resonance is around $9\,\mathrm{Hz}$, and the third resonance is around $14\,\mathrm{Hz}$. These three resonances are the same as the experimental results. The unsprung mass frequency characteristic has one resonance around $13\,\mathrm{Hz}$. This characteristic is also the same as the experimental vehicle.

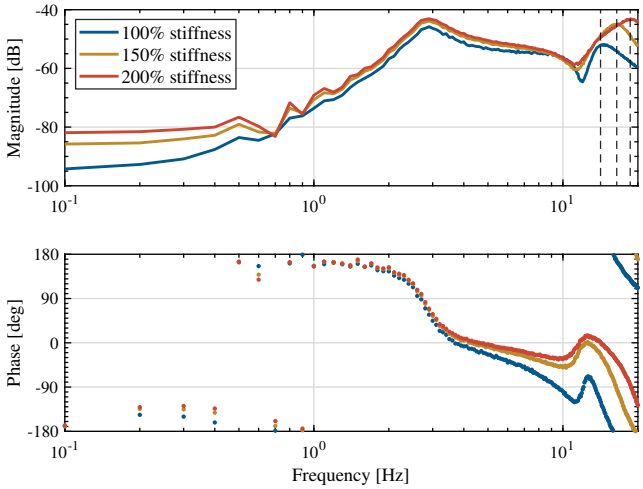

Fig. 12. Comparison of frequency response between bushing stiffness.

By using a multibody dynamics model, it is shown that the third resonance of acceleration can be captured. It essentially comes from the bushing stiffness between the body and the upper arm, lower arm and rod. A sensitivity analysis of this parameter is further performed in the following section in order to quantify and qualify its effects on the frequency response.

C. Sensitivity analysis of bushing coefficient

In this section, we show the sensitivity analysis of the frequency response against the bushing stiffness. Bushing stiffness changes according to deterioration because of environmental changes, such as heat and light. Bushing stiffness increases by 50–120% after vehicles travels $100\,000\,\mathrm{km}$ [18].

The influence of the bushing stiffness is pictured in Fig. 12. It is set from its reference value to 150% and 200% of this value. It can be shown that the higher the bushing stiffness, the higher the third resonance of vibration; explicitly going from $14\,\mathrm{Hz}$ to $19\,\mathrm{Hz}$.

V. Feedforward Controller Design for the Third Resonance Suppression

Therefore, one can conclude on the need to consider the bushing stiffness variation in the design of the motion controller. In other words, the lifetime of this component needs to be taken into account carefully when designing the control algorithms.

We design a feedforward controller for vibration suppression of the third resonance as a simple example. If we apply

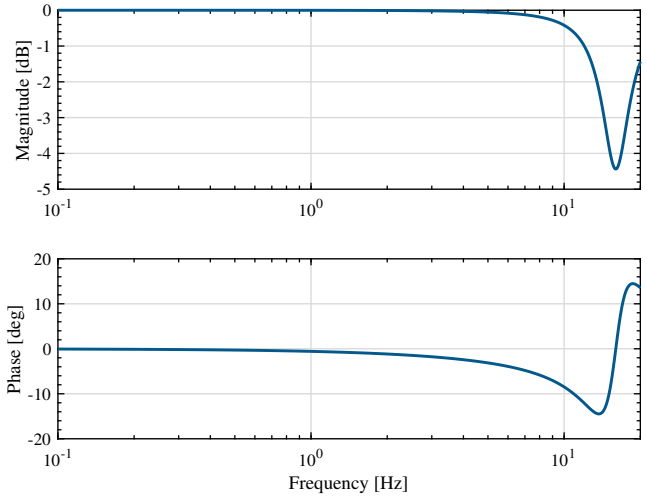

Fig. 13. Notch filter for third resonance suppresstion.

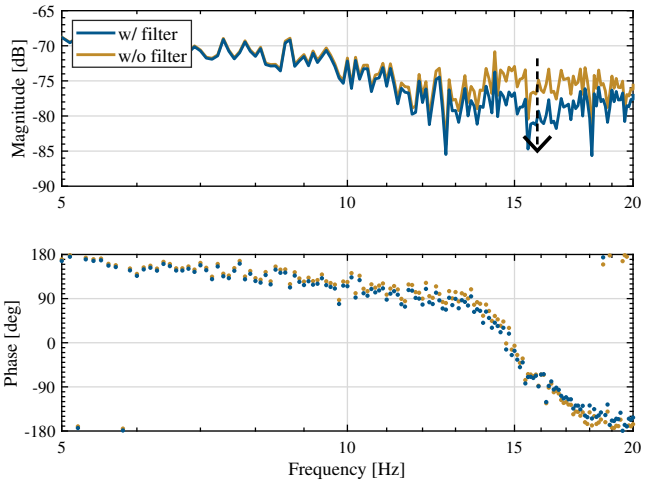

Fig. 14. Sprung mass acceleration with motor torque step input.

the notch filter which covers the third resonance fluctuation as shown in Fig. 13, we can suppress the sprung mass vertical acceleration of the third resonance with motor torque step input as shown in Fig. 14.

VI. Conclusion

In this paper, the frequency response characteristics from IWM torque to sprung mass vertical acceleration was analyzed in order to design the controller for comfortable motion control. Experimental results showed three particular resonance of vibration from which the two lowest can be captured by the classical quarter car model. A multibody dynamics model of the experimental vehicle was developed and allowed to capture the third resonance. It was highlighted that this particular third resonance comes from bushing stiffness and that its frequency value directly depends on the bushing stiffness value. Lastly, the authors show a simple feedforward controller design example based on the model analysis.

Acknowledgment

The author would like to acknowledge the support of the European Commission through Horizon 2020 Research and Innovation Programme (H2020-MSCA-RISE-2016) under the Marie Sklodowska-Curie grant agreement No 734832.

References

[1] Y. Hori, "Future Vehicle Driven by Electricity and Control-Research on Four-Wheel-Motored "UOT Electric March II"," *IEEE Transactions on Industrial Electronics*, vol. 51, no. 5, pp. 954–962, 2004.

[2] K. Sung, T. Nishino, and M. Takayasu, "A power-assistance system using a battery and an electric double-layer capacitor bank for light electric vehicles," *IEEJ Journal of Industry Applications*, vol. 8, no. 3, pp. 465–470, 2019.

[3] M. Bezha and N. Nagaoka, "Improved ann for estimation of power consumption of ev for real-time battery diagnosis," *IEEJ Journal of Industry Applications*, vol. 8, no. 3, pp. 532–538, 2019.

[4] H. Fujimoto, N. Takahashi, A. Tsumasaka, and T. Noguchi, "Motion control of electric vehicle based on cornering stiffness estimation with yaw-moment observer," in *International Workshop on Advanced Motion Control, AMC*, vol. 2006, 2006, pp. 206–211.

[5] S. Murata, "Innovation by in-wheel-motor drive unit (in Japanese," *Vehicle System Dynamics*, vol. 50, no. 6, pp. 807–830, 2012.

[6] V. Ivanov, D. Savitski, J. Orus, J. M. R. Fortun, A. Sorniotti, and P. Gruber, "All-wheel-drive electric vehicle with on-board motors: Experimental validation of the motion control systems," *IECON 2015 - 41st Annual Conference of the IEEE Industrial Electronics Society*, pp. 1729–1734, 2015.

[7] J. M. Rodriguez, R. Meneses, and J. Orus, "Active vibration control for electric vehicle compliant drivetrains," *IECON 2013 - 39th Annual Conference of the IEEE Industrial Electronics Society*, pp. 2590–2595, 2013.

[8] E. Katsuyama, "Decoupled 3D moment control for vehicle motion using In-Wheel motors," *SAE International Journal of Passenger Cars - Mechanical Systems*, vol. 6, pp. 137–146, 2013.

[9] N. Ochi, H. Fujimoto, and Y. Hori, "Proposal of roll angle control method using positive and negative anti-dive force for electric vehicle with four in-wheel motors," *2013 IEEE International Conference on Mechatronics, ICM 2013*, pp. 816–821, 2013.

[10] M. Liu, F. Gu, and Y. Zhang, "Ride comfort optimization of in-wheelmotor electric vehicles with in-wheel vibration absorbers," *Energies*, vol. 10, no. 1647, pp. 1–21, 2017.

[11] V. Roel, B. Igo, and H. Nijmeijer, "Influence of in-wheel motors on the ride comfort of electric vehicles," *Int. Symposium on Advanced Vehicle Control (AVEC)*, pp. 835–840, 2010.

[12] A. Martyn and H. Damian, "Unsprung mass with in-wheel motors-myths and realities," *Int. Symposium on Advanced Vehicle Control (AVEC)*, pp. 261–266, 2010.

[13] E. Katsuyama and A. Omae, "Improvement of Ride Comfort by Unsprung Negative Skyhook Damper Control Using In-Wheel Motors," *SAE International Journal of Alternative Powertrains*, vol. 5, no. 1, pp. 2016–01–1678, 2016.

[14] S. Ohno and K. Ito, "Unsprung vibration control for in-wheel-motor EV," *JSAE Autumn Congress 2014*, no. 103, pp. 21–24, 2014.

[15] H. Fukudome, "Reduction of longitudinal vehicle vibration using In-Wheel motors," *SAE Technical Paper Series*, 2016.

[16] A. Takesaki, M. Kawafuku, M. Iwasaki, and T. Fujii, "Vibration Suppression Control System for Electric Vehicle Considering Longitudinal Vibration," *Proc. of IEEJ Technical Meeting Record*, vol. 97, pp. 7–12, 2010.

[17] R. Pintelon, P. Guillaume, Y. Rolain, J. Schoukens, and H. Van Hamme, "Parametric identification of transfer functions in the frequency domain-a survey," *IEEE Transactions on Automatic Control*, vol. 39, no. 11, pp. 2245–2260, 1994.

[18] H. C. Cho and S. H. Lee, "Study on the Long-Term Aging-Resistance of Anti-Vibration Rubber in the Vehicle," *SAE Transactions*, vol. 111, pp. 527–533, 2002.